Plasmonics (2022) 17:2473–2481
https://doi.org/10.1007/s11468-022-01719-3

Refractive Index Sensor Based on Surface Plasmon Resonance Excitation in a D-Shaped Optical Fiber Coated by Tantalum

Nader Sobhkhiz Vayghan[1] · Behrooz Eftekharinia[2]

Received: 2 August 2022 / Accepted: 10 October 2022 / Published online: 9 November 2022

Abstract

In this paper, a plasmonic refractive index sensor using a D-shaped optical fiber coated by tantalum has been proposed. The interaction between fiber fundamental mode and plasmonic mode which lead to the formation of resonance peaks depending on the analyte refractive index (RI) is investigated in detail. Using spectral sensitivity methods, the sensing performance of the proposed sensor for detecting analytes is numerically studied. The effect of various design parameters of proposed sensor is optimized numerically to achieve the maximum wavelength sensitivity. The proposed D-shaped optical fiber sensor has a RI detection range of 1.30 to 1.43 and exhibits a non-linear increasing spectral sensitivity from 1300 to 3900 nm/RIU. The proposed RI sensor is attractive for detecting different RI chemical and biochemical samples due to simple design, relatively large detection range, cost-effective, non-toxic nature, and highly corrosion resistivity plasmonic material.

Keywords D-shaped fiber sensor · Tantalum · Surface plasmon resonance · Refractive index sensor · Plasmonic sensor

Introduction

The surface plasmon resonance (SPR) has been emerged as an advance effective technique in numerous sensing applications that need highly accurate detection of optical refractive index (RI) [1, 2]. In an SPR technique, sensitive detection of RI benefits from the inherent property that necessary parameters for excitation of plasmon polaritons at the metal-dielectric interface like angle of incidence and the resonance wavelength depend strongly on the RI of surrounding medium [3]. SPR-based sensors find its application in various fields such as biological [4] and chemical analyte detection [5], medical diagnostics [6, 7], biochemistry [8], environmental monitoring, food testing, salinity measurement, and antibody-antigen interaction [9–13].

Conventional configuration for SPR sensors is based on Otto and Kretschmann-Raether prism geometries that direct p-polarized light into a glass prism coated with a metal layer and excites plasmonic wave at the metal/analyte interface when the phase matching condition is met at specific parameters of electromagnetic wave incident angle and wavelength [14]. The optical mechanism behind the operation of conventional SPR sensors is attenuated total reflection (ATR) and evanescent waves [15]. Although prism-based SPR sensors perform effectively in RI detection of unknown analyte bordering the metal layer, they are bulky and mechanically unstable for remote sensing applications [16–18].

Over the past decade, motivated by the need of scaling down the sensor size, researchers have designed a large variety of optical fiber–based SPR sensors [9–11]. Fiber-based SPR sensors utilize the improved form of prism-based Kretchmann configuration enabling coupling between optical modes and surface plasmon polaritons (SPPs). Compared with prism-based sensors, fiber-based sensors have small size, high sensitivity, compactness, and light weight. Moreover, they offer high degree of integration and support remote sensing capabilities. In recent years, considerable attention has been devoted to developing D-shaped fiber sensors driven by the need to overcome drawbacks related to fragility after uncladding the usual structure of optical fibers. In fact, uncladding of fiber enhances the sensitivity of the fiber sensor. However, it will become more fragile for continuous monitoring [19, 20]. In these new structures, the surface of fiber is polished in

✉ Nader Sobhkhiz Vayghan
nsobhkhiz@aeoi.org.ir; n.sobhkhiz@modares.ac.ir

Behrooz Eftekharinia
b.eftekharinia@nit.ac.ir

[1] Photonics and Quantum Technology Research School, Nuclear Science and Technology Research Institute, AEOI, Tehran 1339-14155, Tehran, Iran

[2] Department of Physics, Faculty of Basic Science, Babol Noshirvani University of Technology, Babol, Mazandaran, Iran

a D-shape and deposited by metal to excite plasmonic wave and monitor the interaction between the evanescent wave and the surrounding medium and detecting small changes in RI in this medium [21–24].

Until now, different plasmonic metals have been proposed to enhance the sensitivity of fiber-based SPR sensors, including silver (Ag), gold (Au), and aluminum (Al). Silver exhibits high sensitivity and sharp resonance peaks in UV-vis range of electromagnetic spectrum [25]. Unfortunately, it suffers from an oxidation issue which hinders its stable applicability. Attempts have been devoted to increase the sensitivity and stabilization of Ag by deposition additional layers such as graphene or TiO_2 [26–28]. But this increases fabrication costs and complexity. Al is another strong candidate metal for plasmonic sensors owing to its high electron density and relative low damping loss but its application is also hindered by oxidation problem. Although Au has been used widely in various sensing applications due to its sensitivity and stability, deposition of it throughout the polished surface in fiber-based SPR leads to the wastage of precious metal [29].

Tantalum (Ta), a transition metal on the periodic table, has been emerged as a promising refractory metal to extend the plasmonic technique into the IR wavelengths. Because of large dumping factors in dielectric functions of most metals at the IR range, development of tunable plasmonic in this region is challenging. The plasmonic tuning at the IR regions has been reported by using tantalum nanoparticle [30]. Due to its non-toxic nature and highly corrosion resistivity, Ta has been utilized in surgical implants and capacitors. Moreover, it is compatible with physical vapor deposition techniques and can be utilized in optical coatings, magnetic storage media, wear, and corrosion-resistant coatings. With these properties, Ta is considered to bring new possibilities of optoelectronic applications over IR range including plasmonic SPR sensors.

In this paper, we investigate the deposition of tantalum nanofilm on a simple D-shaped optical fiber and study the RI sensing performance of the sensor in detail. To the best of our knowledge, this is the first time that Ta nanofilms are being investigated in optical fiber–based SPR sensors with simple D-shaped structure for detecting analytes. We demonstrate the superior characteristics of our proposed sensor to detect analytes with RI between 1.30 and 1.43. We will also study the effect of design parameters on the performance of the proposed sensor. For this purpose, we acquire a waveguide-coupled SPR method using an FEM technique.

Methods and Device Structure

The cross-sectional view of the designed plasmonic-base D-shaped fiber sensor is shown in Fig. 1a. The diameters of fiber core and cladding are taken as 8.2 and 125 μm, respectively, to satisfy single mode fiber (SMF) conditions. The fabrication process of D-shaped fibers involves a well-known and mature side-polishing technique combined with an improved motor-driven technique to suspend the fiber and control the polishing depth [31, 32]. An accurate polishing process is controlled by a photometer connected with a monitoring computer system. The polishing depth can be controlled by controlling polishing time.

The designed D-shaped fiber can be used in experimental setup of Fig. 1b for sensing purposes which includes a white light source with an optical spectrum analyzer (OSA) to monitor the output response propagated through the proposed sensor. Both ends of proposed sensor are spliced with SMF of diameter 125 μm using a fusion splicer and the sensing head is immersed in liquid. This configuration of sensing system using all-in-fiber shows the strong mechanical reliability and is easy to operate in remote sensing. It is expected that when the SPR phenomenon takes place, a sharp transmission peak will be observed on OSA.

The Ta strip is considered as the plasmonic material deposited over the fiber core to enhance its sensitivity. The Ta layer can be coated on the polished surface by using magnetron sputtering or electron beam evaporation techniques. Complex refractive index used for Ta material in our simulation is represented in Fig. 2 [33].

We used GeO_2-doped silica and fused silica as traditional materials for fiber core and cladding, respectively, and Sellmeier's equation is used for description of material dispersion as follows [34]:

$$n^2(\lambda) = 1 + \frac{B_1\lambda^2}{\lambda^2 - C_1} + \frac{B_2\lambda^2}{\lambda^2 - C_2} + \frac{B_3\lambda^2}{\lambda^2 - C_3}. \quad (1)$$

where n denotes the wavelength λ dependence of RI for both core and cladding and $B_{1,2,3}$ and $C_{1,2,3}$ are Sellmeier's coefficients whose values are given in Table 1.

For characterization and optimization of the proposed sensor performance, a finite element technique [35] based on COMSOL Multiphysics Software (Version 5.6) is used. To this end, energy coupling between core mode and SPP mode is investigated by using coupled mode theory [36]. A two-dimensional (2D) modal analysis is carried out on x and y directions. Electromagnetic wave with frequency domain is selected for the physics of simulation and specified parameters were defined as defaults in mode analysis. Important parameters of the designed system include the width (`w_Ta`), and the thickness (`t_Ta`) of Ta strip, and the analyte RI (n_a). The wavelength λ and n_a are varied in range 1.3–1.8 μm and 1.30–1.43, respectively. After drawing geometry and adding materials to the model, a fine mesh with maximum mesh size of 20 nm is considered in order to achieve the maximum simulation accuracy. Finally, the simulation is run and obtained data and results are analyzed. The energy of fiber mode couples to

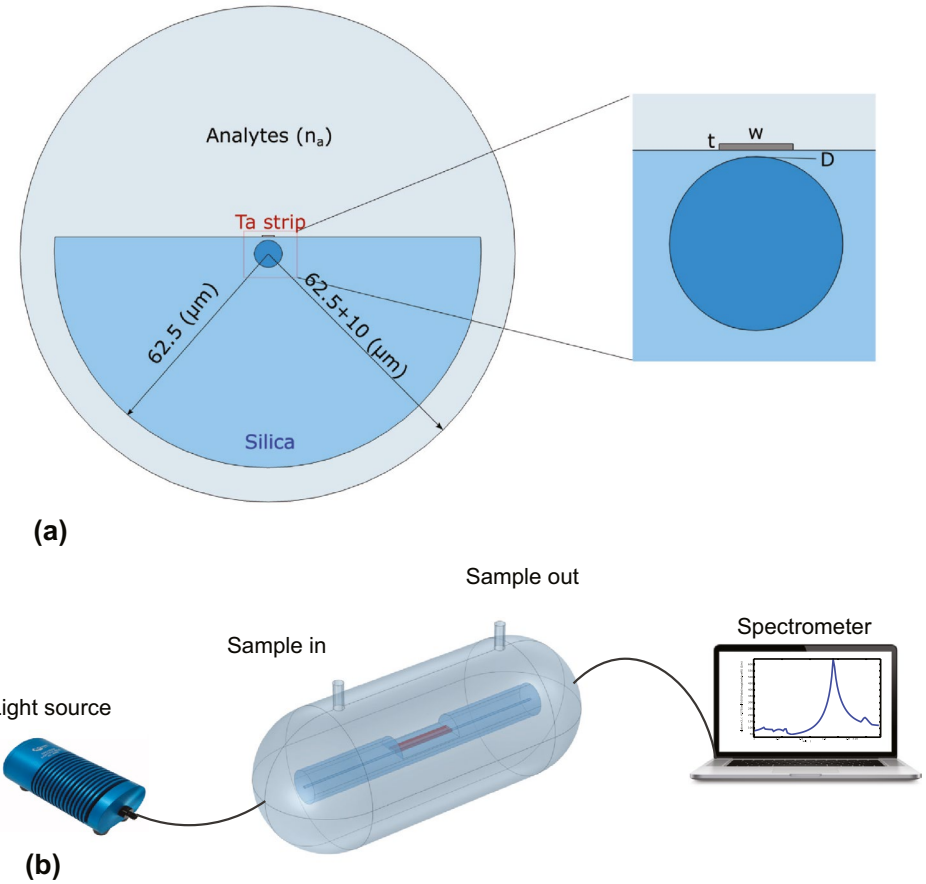

Fig. 1 **a** Schematic of the cross-sectional view of the proposed D-shaped single mode optical fiber sensor. **b** Schematic diagram of experimental setup of proposed D-shaped optical fiber–based SPR sensor

the SPP wave on the Ta surface when the n_{eff} of core-guided mode and SPP mode attain the same propagation constant for resonance wavelength (λ_R). At this wavelength, energy of core-guided mode is highly lost. The confinement loss calculation formula is given in the following equation [37]:

$$\alpha = 40\pi \frac{Im(n_{eff})}{(ln(10)\lambda)} = 8.686 \times k_0 \times Im(n_{eff}) \times 10^4 dB/cm. \quad (2)$$

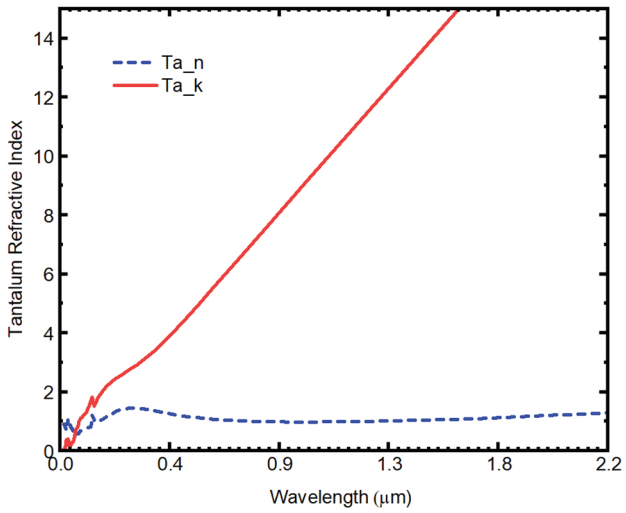

Fig. 2 The real (red curve) and imaginary (dashed blue curve) part of Ta complex refractive index as a function of wavelength [31]

Figure 3 shows simulation results for the variations in the real part of the effective refractive index ($Re(n_{eff})$) for core fundamental mode, and plasmon polariton mode, as well as confinement loss curve as a function of wavelength. This helps to understand the physics behind the coupling mechanism between fiber fundamental mode and plasmonic mode inside a SPR-based D-shaped structure. Because of dispersion properties of optical materials, effective index mode of fundamental mode and SPP mode decrease with different rates as the incident wavelength changes. Therefore, there is a specific wavelength at which the n_{eff} values for fiber mode and plasmonic mode intersect each other.

In our simulation, these values are matched at the operating wavelength 1.57 μm, for the analyte refractive index $n_a = 1.38$. At this point, known as phase matching condition, the resonance phenomenon takes place and core mode (the red dashed curve) and plasmonic mode (the blue dashed curve) in Fig. 3 get coupled with each other. This results

Table 1 $B_{1,2,3}$ and $C_{1,2,3}$ coefficients used in Sellmeier's equation to determine the RI of core and cladding

Material	B_1	B_2	B_3	C_1	C_2	C_3
Fused silica	0.6961663	0.4079426	0.8974794	0.0684043	0.1162414	9.896161
GeO_2-doped silica	0.7345739	0.4271083	0.8270340	0.0869769	0.1119519	10.48654

in a sharp peak in confinement loss spectra of the guiding mode in designed sensor (the black solid curve) in Fig. 3. It is needed to note that more intense plasmonic modes result in sharper peaks in confinement loss spectra and higher sensor sensitivity.

It is noticeable in Fig. 3 that the real parts of effective index curves demonstrate a reverse leap near the loss resonance wavelength. This is a known phenomenon and has been reported, previously [38]. In fact, for D-shaped fibers, the electromagnetic field penetrates more into the cladding with increasing the wavelength, which leads to reduction in real part of effective mode index. At wavelengths around the resonance condition, free electrons and electromagnetic field are influenced by the evanescent field and oscillation of resonant electrons, respectively. As a result, the slow electromagnetic field on the left of the resonant wavelength is accelerated by the resonance. On the other hand, the fast electromagnetic field on the right of the resonant wavelength is decelerated by the resonance. This is the physics behind the dramatic change of the real part of effective index for fiber core mode, and SPP mode appeared around the resonance wavelength.

The three electric field distributions in Fig. 3 illustrate the optical field distribution for core-guided mode (I), SPR mode (II), and the phase-matched mode (III). As shown, the field distribution is uniform across the fiber core and plasmonic mode is excited at resonance condition near the Ta strip. A noticeable decrement in intensity of field distribution is observed at the phase-matching condition since the fiber mode energy is transferred to the plasmonic surface waves for establishment of strong energy coupling at the interface between the Ta plasmonic strip and analyte medium.

The most important structural parameters influencing SPP mode near the metal and dielectric interface are the strip thickness, `t_Ta`, the strip width, `w_Ta`, and the polishing depth, D. Optimization of these parameters is needed since they affect the EM energy of SPP wave reaching the strip-analyte interface.

To this end, we firstly optimized D parameter as it is the most important factor in systematic design of D-shaped fibers. Figure 4a shows simulation results for confinement loss versus incident light wavelength for different D values. As shown, the confinement loss is maximized at 634 dB/cm, $\lambda = 1.57\mu m$ for D = 0. Practical structure of a fiber sensor with this polishing depth to the core could be achieved by a simple combination of mechanical and chemical etching methods [39].

Moreover, it is important to carry out a detailed study on tantalum strip and their influence on the proposed sensor performance since plasmonic mode behavior is influenced strongly by metal layer thickness. For optimization of strip thickness, other structural parameters including D, `w_Ta`, and n_a are kept at constant values, 0 μm, 3.5 μm, and 1.38 respectively.

Figure 4b shows simulation results for confinement loss variations for different values of `t_Ta`. It is shown that the resonance peak corresponding to the maximum confinement

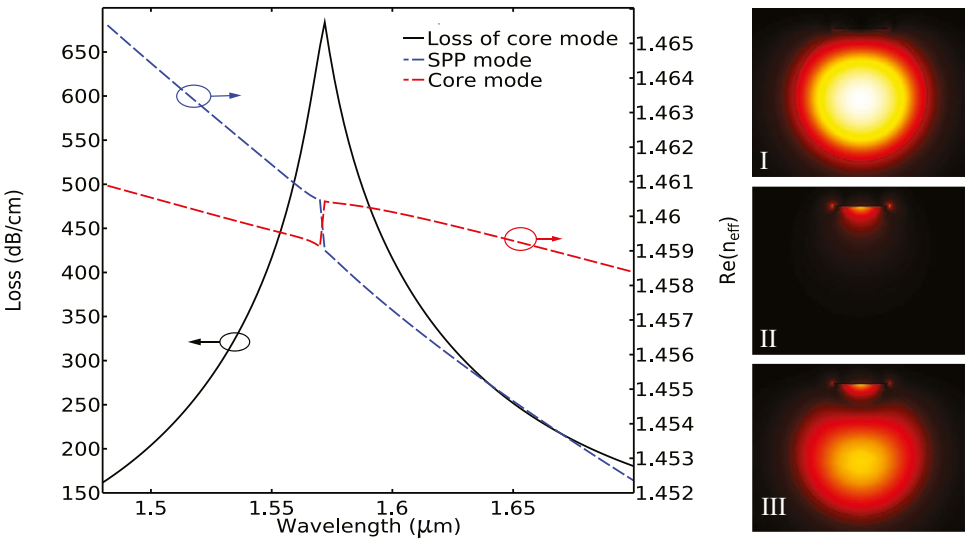

Fig. 3 Dispersion relation of core-guided mode (red dashed line) and SPP mode (blue dashed line) along with confinement loss spectra (black solid line), the right side figures show the mode profiles for (I) core-guided mode (II) SPP mode core-guided mode (III) phase-matched mode. Note that the design parameters are $n_a = 1.38$, $D = 0\ \mu m$, $w\_Ta = 3.5\ \mu m$, and $t\_Ta = 50\ nm$

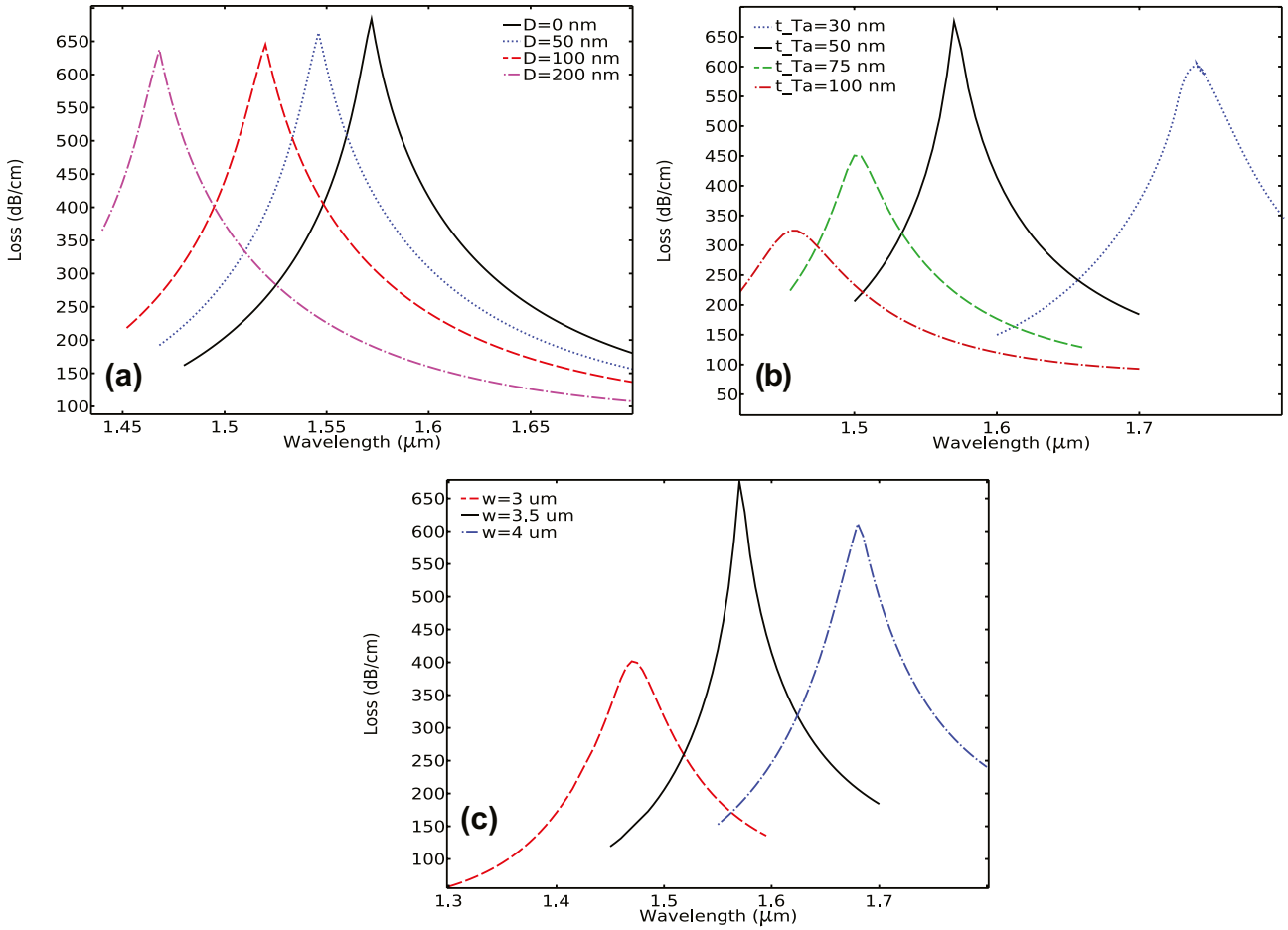

Fig. 4 Confinement loss variation versus wavelength for different values of **a** polishing depth, D, **b** strip thickness, *t_Ta*, and **c** strip width (*w_Ta*)

loss experienced a blue shift when the thickness of the Ta strip increased from 30 to 100 nm. This blue shift in resonance wavelength, λ_R, is ascribed to variation in n_{eff} of SPP mode when strip thickness changes. From the simulation results, the resonance conditions occurred for $\texttt{t\_Ta} = 50$ *nm* and in the following simulations, we consider it as the optimized value of strip thickness.

Figure 4c shows the variation of confinement loss as a function of wavelength for three different values of `w_Ta`, to see the effect of strip width on performance of the sensor. It is found that a maximum spectral loss of 634 dB/cm is obtained for $\texttt{w_Ta} = 3.5\ \mu$m. As shown, we used structural optimization of sensor design to find the phase-matching point at which the spectral loss reaches its maximum intensity. This results in easier and more efficient detection using a fiber sensor.

We have then investigated the sensor response for a wide range of RI varying between 1.30 and 1.43. Figure 5a, b exhibits the detailed comparison of confinement loss as a function of wavelength for two ranges of RI of analytes, i.e., 1.30–1.36 and 1.37–1.43 respectively. Here, from graphs, we may clearly observe that Fig. 5a has less wavelength shift than Fig. 5b. The larger wavelength shift means higher wavelength sensitivity [40, 41].

It was founded that the resonance wavelength at which the confinement loss reaches its maximum experiences a red shift with increment of analyte RI. In addition, the confinement loss peak intensity decreases when RI value of the analyte increases. In fact, when n_a increases to values near the fiber RI, mode coupling between the core mode and plasmonic wave reduces. Moreover, it leads to broadening of confinement loss spectra.

Figure 6 plots variation of resonance wavelength and sensitivity of the designed sensor versus n_a of the analyte. It represents a good polynomial fitting between resonance wavelength and n_a. Using this polynomial fitting, we calculated the sensitivity factor of the designed sensor according to the following equation [42]:

$$S_\lambda = d\lambda_{peak}/dn_a \frac{nm}{RIU}. \tag{3}$$

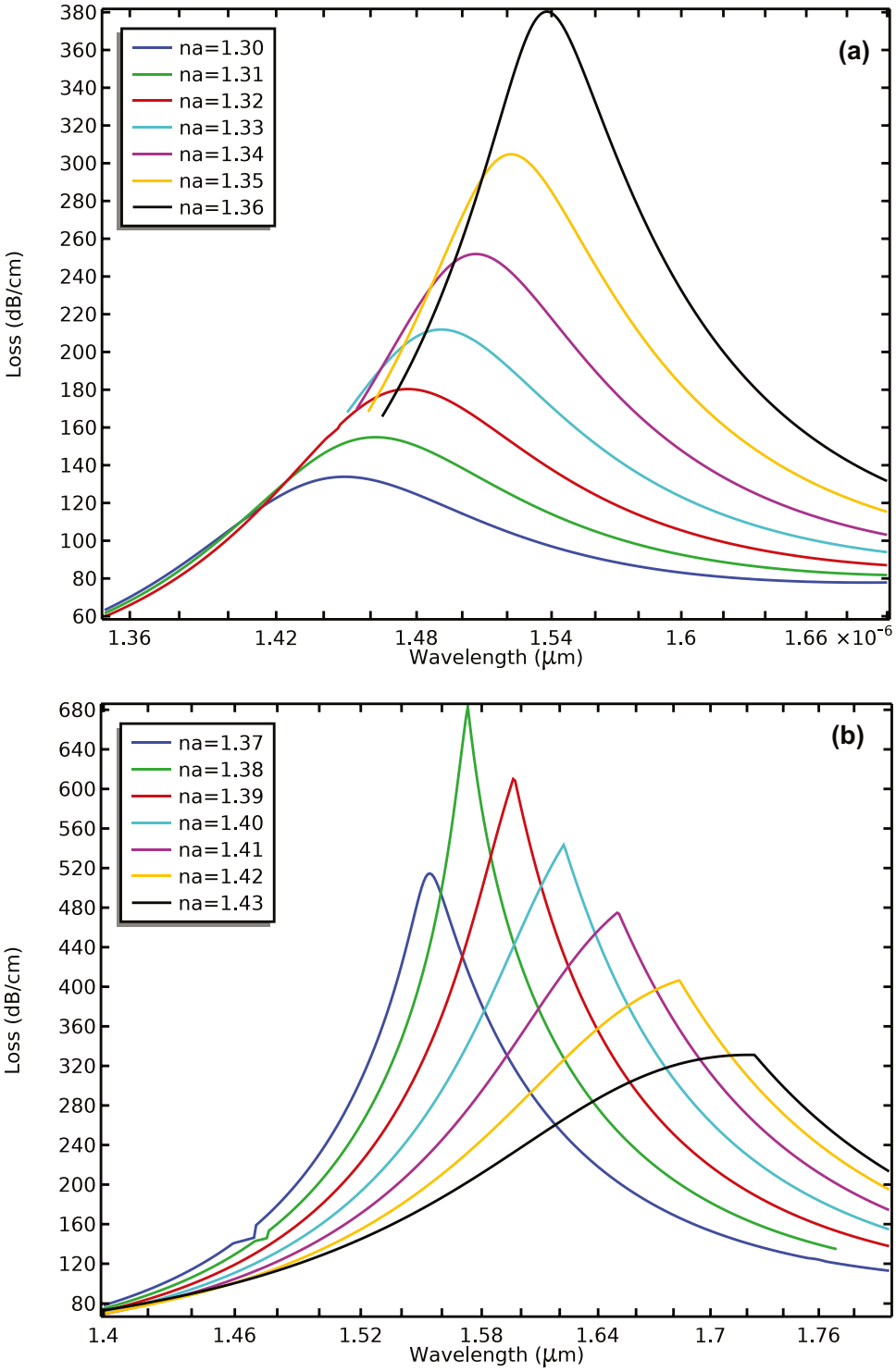

Fig. 5 Confinement loss spectra of the designed sensor for na of analytes in range of **a** 1.30 to 1.36 and **b** 1.37 to 1.43

In the abovementioned equation, $d\lambda_{peak}$ denotes the difference in peak wavelength, and dn_a is the difference in n_a. As shown, the sensitivity factor increases non-linearly from 1300 to 3900 *nm/RIU* for $n_a = 1.30$ to $n_a = 1.43$. Moreover, the designed D-shaped fiber sensor represents a maximum sensitivity of 3900 *nm/RIU*. This sensor could be applicable for detection of important chemicals including propyl alcohol, urine glucose, butyl alcohol, isobutyl alcohol, and hexanol as their RI lies between 1.30 and 1.43.

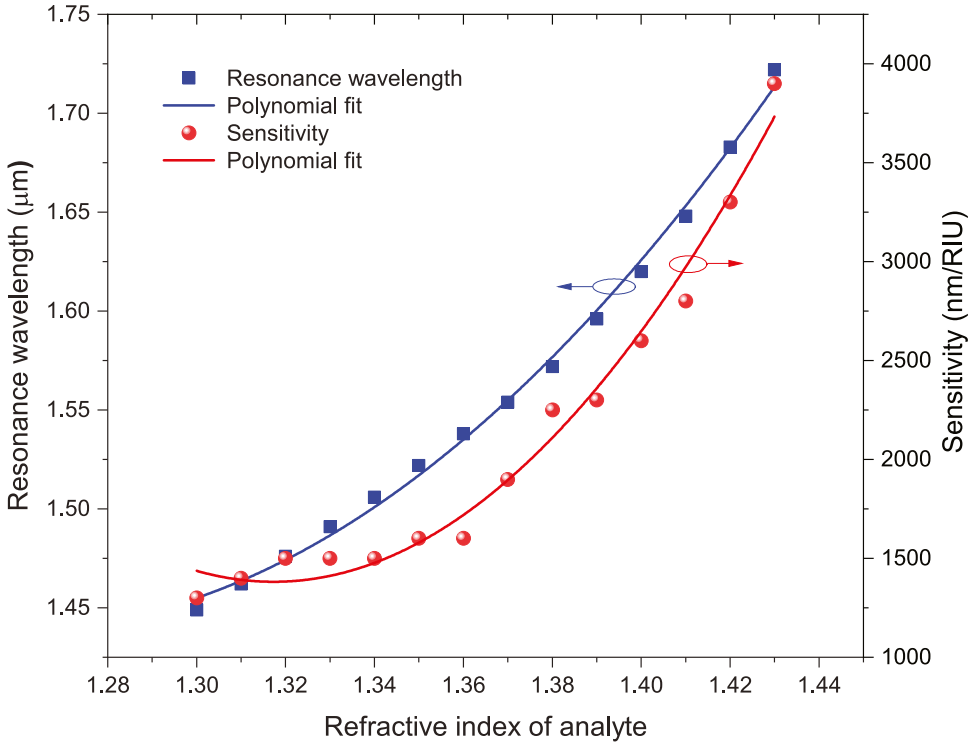

Fig. 6 Variation of the resonance wavelength and sensitivity with the RI of the analyte

Table 2 delivers detailed information about peak loss, resonant wavelength, and wavelength sensitivity for the proposed sensor.

Another factor that describes the ability of optical sensors in detecting small variations in RI of the analyte material is resolution which is calculated according to the following equation [32]:

Table 2 Circumstantial results of the proposed sensor

Refractive index (*RIU*)	Loss (*dB/cm*)	λ_{peak} (*nm*)	Resonant peak shift $\Delta\lambda$(*nm*)	S_λ (*nm/RIU*)
1.3	133.86	1449	13	1300
1.31	154.83	1462	14	1400
1.32	180.34	1476	15	1500
1.33	211.89	1491	15	1500
1.34	251.9	1506	15	1500
1.35	304.77	1522	16	1600
1.36	380.37	1538	16	1600
1.37	514.53	1554	16	1600
1.38	683.23	1573	19	1900
1.39	609.91	1596	23	2300
1.4	543.34	1622	26	2600
1.41	474.81	1650	28	2800
1.42	406.5	1683	33	3300
1.43	331.19	1722	39	3900

$$R = \frac{\Delta\lambda_{min}}{S}. \tag{4}$$

where $\Delta\lambda_{min}$ is the minimum spectral resolution and S is the obtained sensitivity for the D-shaped fiber sensor. Maximum resolution near to 2.564×10^{-5} RIU is obtained for $\Delta\lambda_{min}$ = 0.1 nm and n_a= 1.43. Therefore, the proposed sensor can be utilized to detect small variations of analyte refractive index in order of 10^{-5}.

Finally, figure of merit (FOM) factor of the designed sensor is obtained from the following equation [43]:

$$FOM = \frac{S}{FWHM} RIU^{-1}. \tag{5}$$

where S is the sensitivity and *FWHM* is the full width at half maximum of the desired resonance. *FWHM* values are obtained of 105 nm, 106 nm, 90 nm, and 123 nm, whereas FOM values are obtained of 12.38 RIU^{-1}, 15.09 RIU^{-1}, 28.88 RIU^{-1}, and 31.7 RIU^{-1} for na= 1.30, 1.35, 1.40, and 1.43 respectively.

Table 3 compares the obtained sensitivity for the designed D-shaped fiber sensor in this work with those of other reported sensors. The proposed tantalum-based plasmonic D-shaped fiber sensor has the benefits of a relatively broad detection range, simple design, and high sensitivities compared with other. This introduces the designed sensor in our research as an attractive alternative fiber optic sensor for detection of different chemicals and biochemical materials.

Table 3 Comparison of sensitivity factor calculated for the proposed sensor with sensitivity reported in the previously published articles

Sensing devices	Reported sensitivity (*nm/RIU*)
Copper-graphene-based photonic crystal fiber plasmonic biosensor	2000 (Rifat et al.) [44]
Graphene-based photonic crystal fiber sensor	2520 (An et al.) [45]
Sensitivity enhancement fiber optic sensor using ZnO thin film	3161 (Shukla et al.) [46]
An D-shaped fiber based on a metallic grating	917 (Yan et al.) [47]
Graphene oxide effect on improvement of silver surface Plasmon resonance D-shaped optical fiber sensor	833 (Amiri et al.) [48]
Theoretical assessment of D-shaped optical fiber chemical sensor associated with nanoscale silver strip operating in near-infrared region	3240 (Pathak and Sigh) [20]
Fabrication and simulation studies on D-shaped optical fiber sensor via surface plasmon resonance	2732 (Zakaria et al.) [49]
Investigation of a SPR based refractive index sensor using a single mode fiber with a large D shaped microfluidic channel	1350 (Pathak et al.) [50]
Gold grating assisted SPR based D-shaped single mode fiber	7590 (Khanikar and Singh) [51]
SPR Label-Free Biosensor with Oxide-Metal-Oxide-Coated D-Typed Optical Fiber: a Theoretical Study	6558 (Du et al.) [52]
Our work	3900

Conclusion

A simple D-shaped fiber coated with tantalum is proposed as a plasmonic refractive index sensor. The sensor can detect refractive index (RI) liquid analytes with a detection range of 0.13 RIU, ranging from 1.30 to 1.43. Using a spectral sensitivity method, the resonance wavelength location and amount of confinement loss are numerically calculated. Our studies revealed that the proposed biosensor shows a RI detection range of 1.30 to 1.43 and exhibits a non-linear increasing spectral sensitivity from 1300 to 3900 nm/RIU. We also introduced a figure of merit and compare the performance of our sensor to similar RI sensors based on D-shaped fiber sensor. As our proposed RI sensor has a rather simple structure, cost effective, and its plasmonic metal nontoxic nature and highly corrosion resistivity, it can be an interesting platform for detecting various RI chemical and biochemical samples in chemical, biological, and medical applications.

Author Contribution All the authors have significant contribution in this paper.

Data Availability Data and code of this work will be available from the corresponding author upon reasonable request.

Declarations

Competing Interests The authors declare no competing interests.

References

1. Bhardwaj V, Singh VK (2017) Study of liquid sealed no-core fiber interferometer for sensing applications. Sens Actuators, A 254:95–100
2. Pathak A, Singh V (2020) Theoretical assessment of D-shaped optical fiber chemical sensor associated with nanoscale silver strip operating in near-infrared region. Opt Quant Electron 52(4):1–13
3. Stockman MI (2011) Nanoplasmonics: past, present, and glimpse into future. Opt Express 19(22):22029–22106
4. Liedberg B, Nylander C, Lunström I (1983) Surface plasmon resonance for gas detection and biosensing. Sensors and Actuators 4:299–304
5. Maier SA (2006) Plasmonic field enhancement and SERS in the effective mode volume picture. Opt Express 14(5):1957–1964
6. Chin LC, Whelan WM, Vitkin IA (2010) Optical fiber sensors for biomedical applications. In: Optical-thermal response of laser-irradiated tissue. Springer, pp 661–712
7. Mendez A (2013) Optical fiber sensors for bio-medical applications. In: Optical sensors. Optica Publishing Group, pp SM2D–1
8. Melo AA, Santiago MF, Silva TB, Moreira CS, Cruz RM (2018) Investigation of a D-shaped optical fiber sensor with graphene overlay. IFAC-PapersOnLine 51(27):309–314
9. Gangwar RK, Singh VK (2017) Highly sensitive surface plasmon resonance based D-shaped photonic crystal fiber refractive index sensor. Plasmonics 12(5):1367–1372
10. Wang X, Zhu J, Tong H, Yang X, Wu X, Pang Z, Yang H, Qi Y (2019b) A theoretical study of a plasmonic sensor comprising a gold nano-disk array on gold film with a SiO2 spacer. Chin Phys B 28(4):044201
11. Wang X, Zhu J, Wen X, Wu X, Wu Y, Su Y, Tong H, Qi Y, Yang H (2019) Wide range refractive index sensor based on a coupled structure of Au nanocubes and Au film. Opt Mater Express 9(7):3079–3088
12. Yasli A, Ademgil H (2018) Geometrical comparison of photonic crystal fiber-based surface plasmon resonance sensors. Opt Eng 57(3):030801
13. Yi Z, Liang C, Chen X, Zhou Z, Tang Y, Ye X, Yi Y, Wang J, Wu P (2019) Dual-band plasmonic perfect absorber based on graphene metamaterials for refractive index sensing application. Micromachines 10(7):443
14. Raether H (1988) Surface plasmons on smooth surfaces. Surface plasmons on smooth and rough surfaces and on gratings pp 4–39
15. Otto A (1968) Excitation of nonradiative surface plasma waves in silver by the method of frustrated total reflection. Z Phys A: Hadrons Nucl 216(4):398–410
16. Acimovic SS, Ortega MA, Sanz V, Berthelot J, Garcia-Cordero JL, Renger J, Maerkl SJ, Kreuzer MP, Quidant R (2014) LSPR

chip for parallel, rapid, and sensitive detection of cancer markers in serum. Nano Lett 14(5):2636–2641
17. Ouyang Q, Zeng S, Jiang L, Hong L, Xu G, Dinh XQ, Qian J, He S, Qu J, Coquet P et al (2016) Sensitivity enhancement of transition metal dichalcogenides/silicon nanostructure-based surface plasmon resonance biosensor. Sci Rep 6(1):1–13
18. Wang D, Loo JFC, Chen J, Yam Y, Chen SC, He H, Kong SK, Ho HP (2019a) Recent advances in surface plasmon resonance imaging sensors. Sensors 19(6):1266
19. Klantsataya E, Jia P, Ebendorff-Heidepriem H, Monro TM, François A (2016) Plasmonic fiber optic refractometric sensors: from conventional architectures to recent design trends. Sensors 17(1):12
20. Pathak A, Singh V (2020) Theoretical assessment of D-shaped optical fiber chemical sensor associated with nanoscale silver strip operating in near-infrared region. Opt Quant Electron 52(4):1–13
21. Del Villar I, Zubiate P, Zamarreño CR, Arregui FJ, Matias IR (2017) Optimization in nanocoated D-shaped optical fiber sensors. Opt Express 25(10):10743–10756
22. Liang HQ, Liu B, Hu JF (2017) An ultra-highly sensitive surface plasmon resonance sensor based on D-shaped optical fiber with a silver-graphene layer. Optik 149:149–154
23. Ying Y, Si GY, Luan FJ, Xu K, Qi YW, Li HN (2017) Recent research progress of optical fiber sensors based on D-shaped structure. Opt Laser Technol 90:149–157
24. Zakaria R, Kam W, Ong Y, Yusoff S, Ahmad H, Mohammed WS (2017) Fabrication and simulation studies on D-shaped optical fiber sensor via surface plasmon resonance. J Mod Opt 64(14):1443–1449
25. Naik GV, Shalaev VM, Boltasseva A (2013) Alternative plasmonic materials: beyond gold and silver. Adv Mater 25(24):3264–3294
26. Fu H, Zhang M, Ding J, Wu J, Zhu Y, Li H, Wang Q, Yang C (2019) A high sensitivity D-type surface plasmon resonance optical fiber refractive index sensor with graphene coated silver nanocolumns. Opt Fiber Technol 48:34–39
27. Kadhim RA, Yuan L, Xu H, Wu J, Wang Z (2020) Highly sensitive D-shaped optical fiber surface plasmon resonance refractive index sensor based on Ag-α-Fe 2 O 3 grating. IEEE Sens J 20(17):9816–9824
28. Paul AK, Sarkar AK, Razzak SA (2017) Graphene coated photonic crystal fiber biosensor based on surface plasmon resonance. In: 2017 IEEE Region 10 Humanitarian Technology Conference (R10-HTC). IEEE, pp 856–859
29. Soares M, Rodrigues D, Vidal M, Facão M, Cennamo N, Zeni L, Caucheteur C, Costa F, Leitão C, Pereira S et al (2022) D-shape optical fiber immunosensors based on SPR for cortisol detection: simulation and experimental procedure. Micro-Structured and Specialty Optical Fibres VII, SPIE 12140:67–78
30. Boltasseva A, Atwater HA (2011) Low-loss plasmonic metamaterials. Science 331(6015):290–291
31. Zainuddin NAM, Ariannejad MM, Arasu PT, Harun SW, Zakaria R (2019) Investigation of cladding thicknesses on silver SPR based side-polished optical fiber refractive-index sensor. Results Phys 13:102255
32. Zhang W, Lian Z, Benson T, Wang X, Lou S (2018) A refractive index sensor based on a D-shaped photonic crystal fiber with a nanoscale gold belt. Opt Quant Electron 50(1):1–12
33. Werner WS, Glantschnig K, Ambrosch-Draxl C (2009) Optical constants and inelastic electron-scattering data for 17 elemental metals. J Phys Chem Ref Data 38(4):1013–1092
34. Brückner V (2011) To the use of Sellmeier formula. Senior Experten Service (SES) Bonn and HfT Leipzig. Germany 42:242–250
35. Rahman BA, Davies JB (1984) Finite-element analysis of optical and microwave waveguide problems. IEEE Trans Microw Theory Tech 32(1):20–28
36. Snyder AW (1972) Coupled-mode theory for optical fibers. JOSA 62(11):1267–1277
37. Pathak A, Ghosh S, Gangwar R, Rahman B, Singh V (2019) Metal nanowire assisted hollow core fiber sensor for an efficient detection of small refractive index change of measurand liquid. Plasmonics 14(6):1823–1830
38. Weng S, Pei L, Wang J, Ning T, Li J (2017) High sensitivity D-shaped hole fiber temperature sensor based on surface plasmon resonance with liquid filling. Photonics Research 5(2):103–107
39. Patnaik A, Senthilnathan K, Jha R (2015) Graphene-based conducting metal oxide coated D-shaped optical fiber SPR sensor. IEEE Photonics Technol Lett 27(23):2437–2440
40. Yang X, Lu Y, Duan L, Liu B, Yao J (2017) Temperature sensor based on hollow fiber filled with graphene-Ag composite nanowire and liquid. Plasmonics 12(6):1805–1811
41. Yang X, Lu Y, Liu B, Yao J (2017) Analysis of graphene-based photonic crystal fiber sensor using birefringence and surface plasmon resonance. Plasmonics 12(2):489–496
42. Wu J, Li S, Wang X, Shi M, Feng X, Liu Y (2018) Ultrahigh sensitivity refractive index sensor of a D-shaped PCF based on surface plasmon resonance. Appl Opt 57(15):4002–4007
43. Gangwar RK, Min R, Kumar S, Li X (2021) GeO2 doped optical fiber plasmonic sensor for refractive index detection. Front Phys p 509
44. Rifat AA, Mahdiraji GA, Ahmed R, Chow DM, Sua Y, Shee Y, Adikan FM (2015) Copper-graphene-based photonic crystal fiber plasmonic biosensor. IEEE Photonics J 8(1):1–8
45. An G, Li S, Yan X, Zhang X, Yuan Z, Wang H, Zhang Y, Hao X, Shao Y, Han Z (2017) Extra-broad photonic crystal fiber refractive index sensor based on surface plasmon resonance. Plasmonics 12(2):465–471
46. Shukla S, Sharma NK, Sajal V (2015) Sensitivity enhancement of a surface plasmon resonance based fiber optic sensor using ZnO thin film: a theoretical study. Sens Actuators, B Chem 206:463–470
47. Yan HT, Liu Q, Ming Y, Luo W, Chen Y, Lu Yq (2013) Metallic grating on a D-shaped fiber for refractive index sensing. IEEE Photonics J 5(5):4800706–4800706
48. Amiri IS, Alwi SAK, Raya SA, Zainuddin NAM, Rohizat NS, Rajan MM, Zakaria R (2019) Graphene oxide effect on improvement of silver surface plasmon resonance D-shaped optical fiber sensor. J Opt Commun
49. Zakaria R, Kam W, Ong Y, Yusoff S, Ahmad H, Mohammed WS (2017) Fabrication and simulation studies on D-shaped optical fiber sensor via surface plasmon resonance. J Mod Opt 64(14):1443–1449
50. Pathak A, Singh V, Ghosh S, Rahman B (2019) Investigation of a SPR based refractive index sensor using a single mode fiber with a large D shaped microfluidic channel. OSA Continuum 2(11):3008–3018
51. Khanikar T, Singh VK (2019) Gold grating assisted SPR based D-shaped single mode fiber for detection of liquid refractive index. Opt Quant Electron 51(9):1–10
52. Du B, Yang Y, Zhang Y, Yang D (2019) SPR label-free biosensor with oxide-metal-oxide-coated D-typed optical fiber: a theoretical study. Plasmonics 14(2):457–463